

Renormalization group approach to interfacial motion in incompressible Richtmyer-Meshkov instability

Chihiro Matsuoka*

Department of Physics, Graduate School of Science and Technology, Ehime University, Bunkyocho 2-5, Matsuyama 790-8577, Japan

(Received 24 May 2010; revised manuscript received 2 August 2010; published 24 September 2010)

Nonlinear interfacial motion in incompressible Richtmyer-Meshkov instability is theoretically investigated using the renormalization group approach. The amplitude equation describing the asymptotic interfacial motion is derived using this approach. A comparison with calculations carried out by the weakly nonlinear analysis is performed for various Atwood numbers and the validity of the renormalization group approach is discussed. We show that this approach suppresses the divergence in the perturbative solutions obtained by the weakly nonlinear analysis and provides better approximations for the growth rate of bubbles and spikes and interfacial profiles at the asymptotic nonlinear stage without requiring the use of Padé approximants.

DOI: [10.1103/PhysRevE.82.036320](https://doi.org/10.1103/PhysRevE.82.036320)

PACS number(s): 47.20.Ma, 05.10.Cc, 02.30.Mv, 47.20.Ky

I. INTRODUCTION

The Richtmyer-Meshkov instability (RMI) [1] is a complicated hydrodynamic instability in which both compressibility and incompressibility coexist. RMI is important in various areas such as inertial confinement fusion (ICF), astrophysics [2], and anisotropic turbulent processes [3]. In linear theory, we cannot ignore the compressibility in a system, and therefore, the shock-interface interaction must be taken into account in order to investigate the interfacial motion in RMI [4–6]. However, when the shocks have traveled a distance greater than a wavelength, the system can be regarded as incompressible and irrotational (for weak shocks) except for the interface at which nonuniform vorticity is induced by shocks. Then, we can treat the interface between two fluids as a nonuniform vortex sheet [7,8]. A typical theoretical analysis used for investigating such a nonlinear region is the weakly nonlinear (WN) analysis [6,7,9,10].

Generally, the result of the WN analysis agrees well over a long period with the direct simulation or experimental results when the system is stable, i.e., when the linear solution (lowest order in the analysis) is stable, such as in the case of capillary-gravity waves [11,12]; however, the result considerably deviates from simulations or experimental results [13] when the system is linearly unstable. Zhang and Sohn [9] and Vandenboomgaerde *et al.* [10] carried out the WN analysis (naive perturbations) for the governing equations up to the fourth order and the 11th order, respectively, and investigated the temporal evolution of the interface in RMI. Matsuoka *et al.* [6,7] calculated it up to the third order with a stretched coordinate for the tangential direction of the interface and compared the result with the direct simulation and experimental results. However, these analysis did not suitably describe the velocities of bubbles and spikes at the asymptotic nonlinear stage, and as a result, they required the use of the Padé approximants [7,9] in order to fit the analytical results to the direct simulations or experimental results [13]. The results of these naive perturbations indicate that the amplitude of the interface diverges (at least within the WN analysis) for time $t \gg 1$, t , time, irrespective of how small the

expansion parameter used in the perturbations is, despite the fact that the actual amplitude of the interface in RMI does not diverge. In order to avoid this divergence and improve the approximation in the asymptotic nonlinear stage, we adopt the renormalization group (RG) approach in this paper.

When the system is linearly stable, we can derive the amplitude equation that describes the asymptotic motion of the system. The typical examples of such amplitude equations are the nonlinear Schrödinger equation in water waves [14] or the Newell-Whitehead equation [15] in pattern formation. Usually, these amplitude equations are derived as the secular free condition at higher-order terms in multiple-scale (singular) perturbations to the governing equations. In other words, the existence of secular terms that need to be eliminated is essential for deriving amplitude equations. However, there does not exist such a higher-order secular term in the naive perturbation of RMI. The linear solution of RMI is of a form proportional to time t that is regarded as a secular solution in usual perturbations; therefore, all higher-order terms (including the linear term) become secular within the naive perturbations, i.e., there does not exist a secular term in RMI that can be eliminated. This is because the WN analysis becomes meaningless if we eliminate the (lowest order) linear solution as a secular term. For such an unstable system, we cannot derive the amplitude equation by a conventional multiple-scale method. Instead, we use the RG method here.

The RG method is one of the singular perturbations that removes secular terms from naive perturbations and derive amplitude equations. As stated in Refs. [17,18], the RG approach requires neither specific physical scalings in space and time nor the asymptotic matching performed in the conventional singular perturbation theory. In addition, the RG approach does not require the stability of the linear solution, i.e., we can derive the amplitude equation using this method even if the lowest-order solution in the perturbations is unstable [19,20]. However, the amplitude equations derived by the RG method, called RG equations [16,17], are essentially ordinary differential equations; therefore, we need to calculate Fourier mode expansions beforehand to apply this method to partial differential equations. It is not easy to calculate the higher order RG equations with typical RG approach [16,17,19]. In order to overcome this difficulty, Goto *et al.* introduced a reformulated RG method on the basis of a

*matsuoka@phys.sci.ehime-u.ac.jp

naive renormalization transformation and the Lie group approach [20]. We adopt this reformulated RG method in this paper. Geometrically, the RG equation describes the envelope of a family of initial surfaces [16] and it gives the asymptotic behavior of the system.

In this paper, we derive the RG equation for describing the asymptotic interfacial motion in RMI. The RG equation is an amplitude equation, and therefore, it cannot describe complicated stages such as the mushroomlike structure in RMI; however, it gives the growth rate of bubbles and spikes or interfacial profiles with better accuracy than the WN analysis. In order to investigate the bubble motion for $t \gg 1$, the potential-flow model [21,22] is also effective. This method was first presented by Layzer [23] and applied to the Rayleigh-Taylor instability (RTI). The solution by the potential-flow model approximates well the asymptotic growth rate of a bubble, however, this is a local solution in the neighborhood of a bubble and it cannot describe the interfacial motion away from the bubble. As in the case of the WN analysis, the RG approach gives a global solution to the interfacial motion, therefore, that can describe the asymptotic behavior of spikes as well as bubbles. In Sec. II, we perform the WN analysis up to the fifth order. This calculation becomes the basis for deriving the RG equation. Using the results of the WN analysis, we derive the RG equation in Sec. III. In Sec. IV, we present a comparison of the growth rate of bubbles and spikes between the analytical solutions obtained in Secs. II and III and the numerical calculations for various Atwood numbers. Section V presents the conclusions of this study.

II. WEAKLY NONLINEAR ANALYSIS FOR GOVERNING EQUATIONS

In this section, we carry out the WN analysis for constructing naive perturbative solutions. These solutions also become the basis of the RG approach described in the next section. Here, we consider here a planar case, and therefore, the interface (x, y) can be described by a curve $y = \eta(x, t)$. The governing equations for the stability analysis are the Bernoulli equation (pressure continuous condition) and kinematic boundary conditions (normal velocity continuous condition at the interface),

$$(1 - A) \left\{ \frac{\partial \phi_1}{\partial t} + \frac{1}{2} \left[\left(\frac{\partial \phi_1}{\partial x} \right)^2 + \left(\frac{\partial \phi_1}{\partial y} \right)^2 \right] \right\} = (1 + A) \left\{ \frac{\partial \phi_2}{\partial t} + \frac{1}{2} \left[\left(\frac{\partial \phi_2}{\partial x} \right)^2 + \left(\frac{\partial \phi_2}{\partial y} \right)^2 \right] \right\}, \quad (1)$$

$$\frac{\partial \eta}{\partial t} - \frac{\partial \phi_i}{\partial y} = - \frac{\partial \phi_i}{\partial x} \frac{\partial \eta}{\partial x} \quad (i = 1, 2), \quad (2)$$

where $A = (\rho_2 - \rho_1) / (\rho_1 + \rho_2)$ is the Atwood number, ρ_i ($i = 1, 2$) is the density of fluid i , and the velocity potential ϕ_i is related to the fluid velocity \mathbf{u}_i as $\mathbf{u}_i = \nabla \phi_i$ in each region i . All quantities in Eqs. (1) and (2) are estimated as deviations from $y = 0$. Because the system is assumed to be incompressible, the velocity potential ϕ_i satisfies the Laplace equation $\Delta \phi_i = 0$ in each fluid region i ($i = 1, 2$).

We expand ϕ_i and η with a formal expansion parameter ϵ ($\epsilon \ll 1$) as

$$\phi_i = \epsilon \phi_i^{(1)} + \epsilon^2 \phi_i^{(2)} + \dots, \\ \eta = \epsilon \eta^{(1)} + \epsilon^2 \eta^{(2)} + \dots,$$

where ϕ_i are expanded by taking into account the fact that they are solutions to the Laplace equation

$$\phi_i = \sum_{m=1}^{\infty} \epsilon^m \phi_i^{(m)} \\ = \sum_{m=1}^{\infty} \sum_{l=0}^{[(m+1)/2]} \epsilon^m B_{i,m-2l}^{(m)}(t) e^{\mp(m-2l)ky} \cos(m-2l)kx,$$

where Gauss's symbol $[(m+1)/2]$ denotes the maximum integer that does not exceed $(m+1)/2$, $B_{i,m-2l}^{(m)}(t)$ is the amplitude of the $(m-2l)$ th Fourier mode in the m th order of ϵ , and the sign \mp corresponds to the region $y > 0$ or $y < 0$.

Performing the WN expansions up to the fifth order $O(\epsilon^5)$, we obtain

$$\eta^{(1)} = (B_1 k t + a_0) \cos kx, \\ \eta^{(2)} = \frac{A B_1^2 k^3}{2} t^2 \cos 2kx, \\ \eta^{(3)} = - \left[\frac{(4A^2 + 1) B_1^3 k^5}{24} t^3 + \frac{a_0 B_1^2 k^4}{8} t^2 \right] \cos kx \\ + \left[\frac{(4A^2 - 1) B_1^3 k^5}{8} t^3 - \frac{3a_0 B_1^2 k^4}{8} t^2 \right] \cos 3kx, \\ \eta^{(4)} = - \frac{A^3 B_1^4 k^7}{3} t^4 \cos 2kx \\ + \left[\frac{(2A^3 - A) B_1^4 k^7}{3} t^4 - \frac{2a_0 A B_1^3 k^6}{3} t^3 \right] \cos 4kx, \\ \eta^{(5)} = \left[\frac{(16A^4 + 60A^2 + 1) B_1^5 k^9}{960} t^5 + \frac{a_0 (44A^2 + 1) B_1^4 k^8}{192} t^4 \right] \\ \times \cos kx + \left[\left(-\frac{27A^4}{40} + \frac{3A^2}{16} + \frac{3}{128} \right) B_1^5 k^9 t^5 \right. \\ + a_0 \left(\frac{32A^2 + 15}{128} \right) B_1^4 k^8 t^4 \left. \right] \cos 3kx + \left[\left(\frac{25A^4}{24} - \frac{37A^2}{48} \right. \right. \\ \left. \left. + \frac{7}{128} \right) B_1^5 k^9 t^5 + a_0 \left(\frac{-160A^2 + 35}{128} \right) B_1^4 k^8 t^4 \right] \cos 5kx, \quad (3)$$

where k is the wave number, a_0 is the initial amplitude of the interface, and $k B_1 = v_{lin}$. $v_{lin} = (\rho_1 \delta v_{1y+} - \rho_2 \delta v_{2y+}) / (\rho_1 + \rho_2)$ is the asymptotic linear growth rate in the system [6,7,24]. δv_{1y+} and δv_{2y+} are velocity perturbations behind the reflected and transmitted shocks at $t = 0+$, respectively, and they are uniquely determined from the initial amplitude of

the corrugation and the incident shock intensity. In deriving Eq. (3), we selected the initial amplitude and velocity as

$$\eta(0) = a_0 \cos kx, \quad \frac{\partial \eta}{\partial t}(0) = B_1 k \cos(kx), \quad (4)$$

and dropped the terms proportional to t^2 in $\eta^{(4)}$, and t^2 and t^3 in $\eta^{(5)}$. The results up to the fourth order $\eta^{(4)}$ and the fifth order $\eta^{(5)}$ in Eq. (3) agree with those calculated by Zhang and Sohn [9] and Vandenboomgaerde *et al.* [10], respectively, except for the terms that we dropped (these terms depend on how we choose the initial condition). The derivation of the fifth-order quantities is described in the Appendix.

III. RENORMALIZATION GROUP APPROACH TO INTERFACIAL MOTION

In this section, we present the RG equation for describing the asymptotic motion of the interface. The RG equation is constructed by the naive perturbations derived in the previous section. Now, we set the single-mode amplitude

$$\eta(x, t) = \epsilon \tilde{B}(t) \cos kx, \quad (5)$$

where

$$\tilde{B}(t) = kt\tilde{A}(t), \quad (6a)$$

$$\tilde{A}(t) = (B_1 + \epsilon^2 c_{31} t^2 B_1^3 + \epsilon^4 c_{51} t^4 B_1^5 + \dots) \quad (6b)$$

is the renormalized amplitude that should be determined as the solution to the RG equation derived below, and c_{31} and c_{51} are constants obtained from the coefficients of $\cos kx$ in $\eta^{(3)}$ and $\eta^{(5)}$ in Eq. (3), respectively,

$$c_{31} = -\frac{(4A^2 + 1)k^4}{24},$$

$$c_{51} = \frac{(16A^4 + 60A^2 + 1)k^8}{960}. \quad (7)$$

The RG equation should be determined irrespective of the initial value a_0 , and therefore, we dropped the terms multiplied by a_0 . Solving B_1 with respect to \tilde{A} inversely, we obtain

$$B_1 = \tilde{A}(t) - \epsilon^2 c_{31} t^2 \tilde{A}(t)^3 + \epsilon^4 (3c_{31}^2 - c_{51}) t^4 \tilde{A}(t)^5 + O(\epsilon^6 t^6 \tilde{A}(t)^7). \quad (8)$$

Replacing t in $\tilde{A}(t)$ in Eq. (6b) with $t + \tau$, where τ is a parameter, and substituting B_1 in Eq. (8) into the resulting equation, we obtain

$$\begin{aligned} \tilde{A}(t + \tau) &\equiv G_\tau \tilde{A}(t) \\ &= B_1 + \epsilon^2 c_{31} (t + \tau)^2 B_1^3 + \epsilon^4 c_{51} (t + \tau)^4 B_1^5 + \dots \\ &= \tilde{A}(t) + 2\epsilon^2 c_{31} \tau \tilde{A}(t)^3 + \epsilon^4 (-6c_{31}^2 + 4c_{51}) \tau^3 \tilde{A}(t)^5 \\ &\quad + O(\epsilon^2 \tau^2), \end{aligned}$$

where G_τ denotes a translational group [20]. The RG equation [20,18,25]. up to the fifth order is given as

$$\begin{aligned} \lim_{\tau \rightarrow 0} \frac{A(t + \tau) - A(t)}{\tau} &= \frac{d\tilde{A}}{dt} \\ &= \frac{\partial}{\partial \tau} G_\tau \tilde{A}(t) \Big|_{\tau=0} \\ &= 2\epsilon^2 c_{31} t \tilde{A}(t)^3 - \epsilon^4 (6c_{31}^2 - 4c_{51}) t^3 \tilde{A}(t)^5. \end{aligned} \quad (9)$$

This equation corresponds to the amplitude equation in this system and indicates that $dB_1/d\tau=0$, i.e., the coefficient (original amplitude) B_1 does not depend on the parameter τ [16,17]. Note that $d\tilde{A}/dt$ is $O(\epsilon^2)$, i.e., the temporal variation of the renormalized amplitude \tilde{A} is slow. Because $kB_1 = v_{lin}$, we can also consider that we performed renormalization of the asymptotic linear growth rate v_{lin} by the slowly varying amplitude \tilde{A} . The spirits of the RG approach is presented in Refs. [16–18]. For detailed calculations and examples using the RG equations, see Ref. [20]. The mathematical structure of the RG method is provided in Ref. [25]. Assuming similar form to Eq. (6a), Vandenboomgaerde *et al.* derived an amplitude equation for describing the interfacial motion in RMI in a heuristic manner [26]. Their result differs from our amplitude equation Eq. (9), however, they show that the divergence of the interfacial motion by the naive perturbations at the nonlinear stage can be suppressed by using the solution to their amplitude equation.

In the approximation neglecting the second term on the right-hand side of Eq. (9), we have

$$\tilde{B}(t) = kt\tilde{A}(t) = \frac{kt}{\sqrt{\frac{\epsilon^2(4A^2 + 1)}{12} k^4 t^2 + C}}, \quad (10)$$

where the integral constant C is given by the asymptotic linear growth rate v_{lin} as $1/C = \tilde{A}(0) = v_{lin}/k$. From the form of $\tilde{B}(t)$, we see that the renormalized amplitude $\eta(x, t)$ is given as $\eta(x, t) \sim \epsilon k B_1 t \cos kx$ when time t is small and $\eta(x, t) \sim \sqrt{12/(4A^2 + 1)} (k\epsilon)^{-1} \cos kx$ for large t within this approximation. This solution that $\tilde{B}(t)$ is a constant for large t is different from the asymptotic bubble amplitude $\tilde{B}(t) \sim \log t$ given by the conventional potential-flow model [21,22], although the difference between a constant and $\log t$ is very small for large t . In order to obtain the solution $\tilde{A}(t)$ including the second term on the right-hand side of Eq. (9), we need to calculate Eq. (9) numerically.

When we take the higher-order Fourier modes into consideration, we substitute B_1 in Eq. (8) into $\eta^{(2)}$, $\eta^{(3)}$, ... in Eq. (3) and collect the same modes. Then the renormalized multimode amplitude $\eta \equiv \eta_{multi}$ up to the fifth order is given as

$$\tilde{B}_2(t) = [\tilde{c}_{22} t^2 \tilde{A}(t)^2 + \epsilon^2 (-2\tilde{c}_{22} c_{31} + \tilde{c}_{42}) t^4 \tilde{A}(t)^4 + O(\epsilon^4)],$$

$$\tilde{B}_3(t) = [\tilde{c}_{33} t^3 \tilde{A}(t)^3 + \epsilon^2 (-3\tilde{c}_{33} c_{31} + \tilde{c}_{53}) t^5 \tilde{A}(t)^5 + O(\epsilon^4)],$$

$$\tilde{B}_4(t) = [\tilde{c}_{44} t^4 \tilde{A}(t)^4 + O(\epsilon^2)],$$

$$\tilde{B}_5(t) = [\tilde{c}_{55}t^5\tilde{A}(t)^5 + O(\epsilon^2)],$$

$$\eta_{multi}(x,t) = \epsilon\tilde{B}(t)\cos kx + \epsilon^2\tilde{B}_2(t)\cos 2kx + \epsilon^3\tilde{B}_3(t)\cos 3kx + \epsilon^4\tilde{B}_4(t)\cos 4kx + \epsilon^5\tilde{B}_5(t)\cos 5kx, \quad (11)$$

where c_{31} and c_{51} are given by Eq. (7) and

$$\tilde{c}_{22} = \frac{A}{2}k^3,$$

$$\tilde{c}_{33} = \frac{4A^2 - 1}{8}k^5,$$

$$\tilde{c}_{42} = -\frac{A^3}{3}k^7,$$

$$\tilde{c}_{44} = \frac{2A^3 - A}{3}k^7,$$

$$\tilde{c}_{53} = \left(-\frac{27A^4}{40} + \frac{3A^2}{16} + \frac{3}{128}\right)k^9,$$

$$\tilde{c}_{55} = \left(\frac{25A^4}{24} - \frac{37A^2}{48} + \frac{7}{128}\right)k^9.$$

We compare the single-mode RG solution Eq. (5) and the multimode RG solution Eq. (11) with the WN solution and the numerical results in the next section.

IV. COMPARISON WITH NUMERICAL RESULTS

In this section, we compare the analytical results obtained in the previous sections with the numerical calculations. As stated in Sec. I, the abovementioned incompressible model does not provide particularly good approximations at the linear stage in RMI [5,6]. In order to omit this stage and describe the nonlinear regime, we normalize $x \rightarrow kx$, $y \rightarrow ky$, and $t \rightarrow kv_{lin}t$ with the wave number k and the asymptotic linear growth rate $v_{lin} = O(\epsilon)$ so that the absolute value of the velocity of bubbles and spikes in the analytic solution becomes one at (the normalized) time $t=0$. With these normalizations, we compare the solutions obtained by the RG equation and the WN analysis with the numerical results.

For numerical calculations, we adopt the alternate point quadrature method (Figs. 1–3) and the vortex method with finite regularized parameter δ (Figs. 4 and 5) [8,27]. The former method provides us numerical solutions that are similar to the analytical solutions obtained by Eqs. (1) and (2) with spectral accuracy. On the other hand, the thickness of the interface is taken into account through δ in the latter method, and therefore, the accuracy of calculations is lower than the former one. However, this method better describes experimental results such as the roll-up. It should be noted that the roll-up of the interface does not appear in the high-accurate calculation by the alternate point quadrature method (for details, see Ref. [8]).

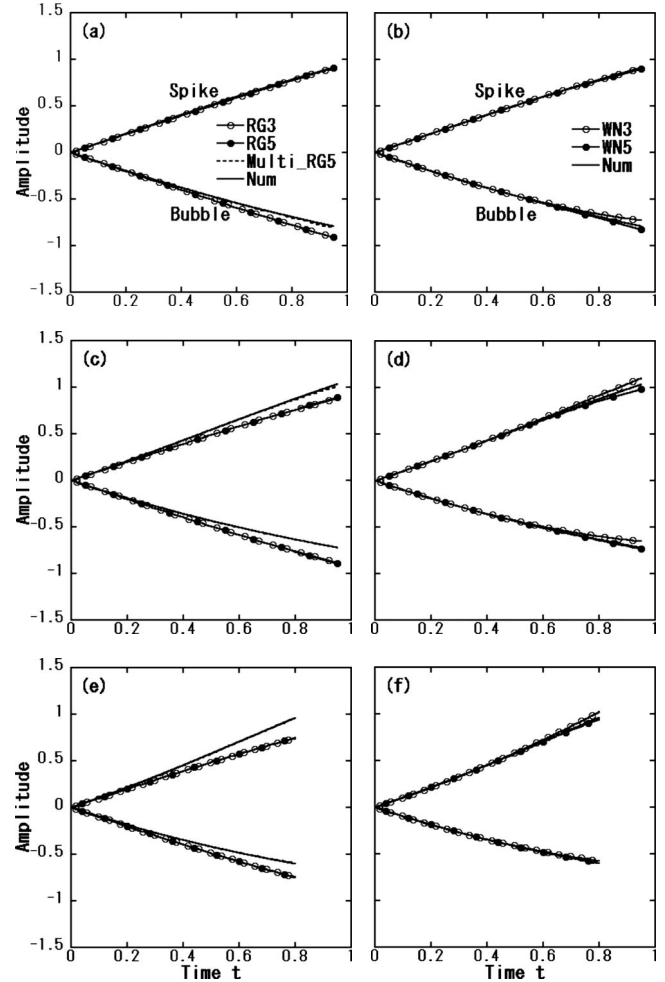


FIG. 1. Comparison of analytical and numerical amplitudes of bubbles and spikes for Atwood number $A=(a)$ and (b) 0.2, (c) and (d) 0.5, and (e) and (f) 0.7, where the time intervals are taken over $0 \leq t \leq 0.95$ for $(a)-(d)$ and $0 \leq t \leq 0.8$ for $(e),(f)$, respectively. The left [(a), (c), and (e)] and right-hand-side figures [(b), (d), and (f)] show the results obtained by the RG equations and the WN analysis, respectively. The solid lines with white and black circles in the left-hand-side figures indicate the results by the third (RG3) and fifth (RG5) orders single-mode RG solutions Eq. (5), and those lines in the right-hand-side figures indicate the results by the third (WN3) and fifth (WN5) orders WN analysis, respectively. The dashed lines in the left-hand-side figures denote the results by the fifth-order multi-mode RG solutions Eq. (11). All solid lines (Num) indicate the numerical results. The numerical calculations in the figure are performed by the alternate point quadrature method with the regularized parameter $\delta=0$.

The grid number, i.e., the number of point vortices N is set to $N=1024$ (Figs. 1–3) and $N=512$ (Figs. 4 and 5) in the numerical calculations by the alternate point quadrature method and the vortex method, respectively. In order to compare the results by the WN analysis and numerical calculations with those by the RG approach, we set $a_0=0$ in the initial condition Eq. (4) for all calculations. Here, the upper fluid ($y>0$) is assumed to be lighter than the lower one ($y<0$).

Figure 1 shows the amplitudes of bubbles and spikes for various Atwood numbers. The final time in each figure cor-

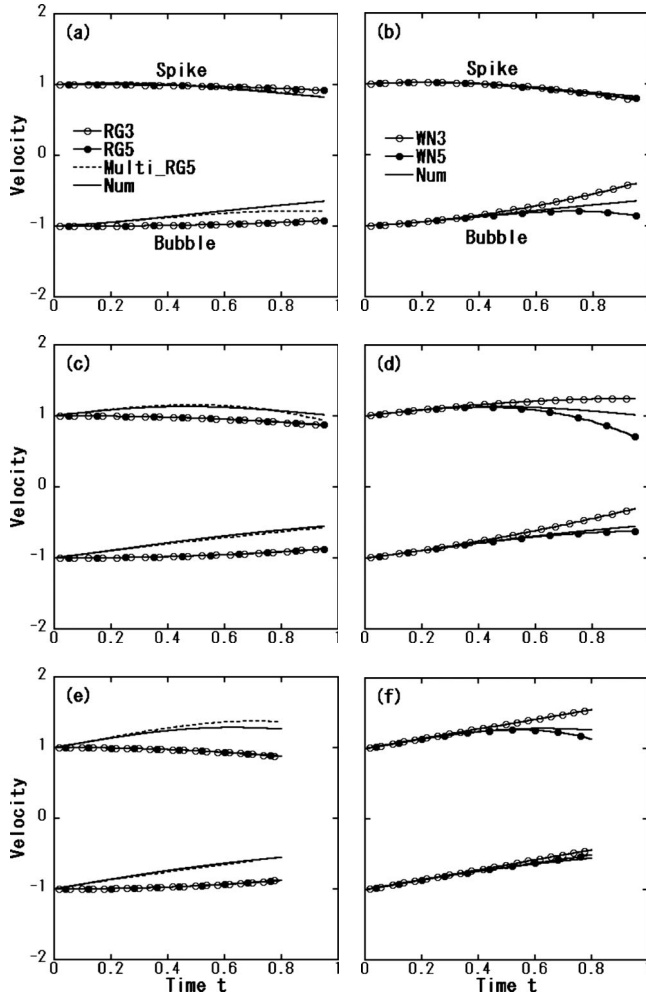


FIG. 2. Velocities of bubbles and spikes for Atwood number A = (a) and (b) 0.2, (c) and (d) 0.5, and (e) and (f) 0.7, where the time intervals and symbols are identical to those in Fig. 1. The numerical calculations in the figure are performed with the same method as in Fig. 1.

responds to the critical time [8] for each Atwood number. After a few time steps of these critical times, Moore's curvature singularity, i.e., the Kelvin-Helmholtz instability [28] occurs and the numerical calculations break down. The symbols RG3 and RG5 in the figure denote the single-mode solution Eq. (5) including up to $O(\tilde{A}(t)^3)$ and $O(\tilde{A}(t)^5)$ on the right-hand side of Eq. (9), respectively, and the symbols WN3 and WN5 denote the solution considering up to the third and fifth orders in the WN analysis given by Eq. (3), respectively. The dashed lines denote the results by the multimode RG solution η_{multi} in Eq. (11) taking into account the term of $O(\tilde{A}(t)^5)$ in Eq. (9). The multimode RG solutions coincide with numerical solutions (at least, on the plot) and we cannot distinguish them for all Atwood numbers. The deviation of the WN solutions from the numerical calculations is smaller than that of the single-mode RG solutions for the amplitudes of bubbles and spikes. As we see from the figure, the difference between the third (RG3) and fifth (RG5) order is very small for the single-mode RG solutions.

We show the velocities (growth rates) of bubbles and spikes for various Atwood numbers in Fig. 2. As for the

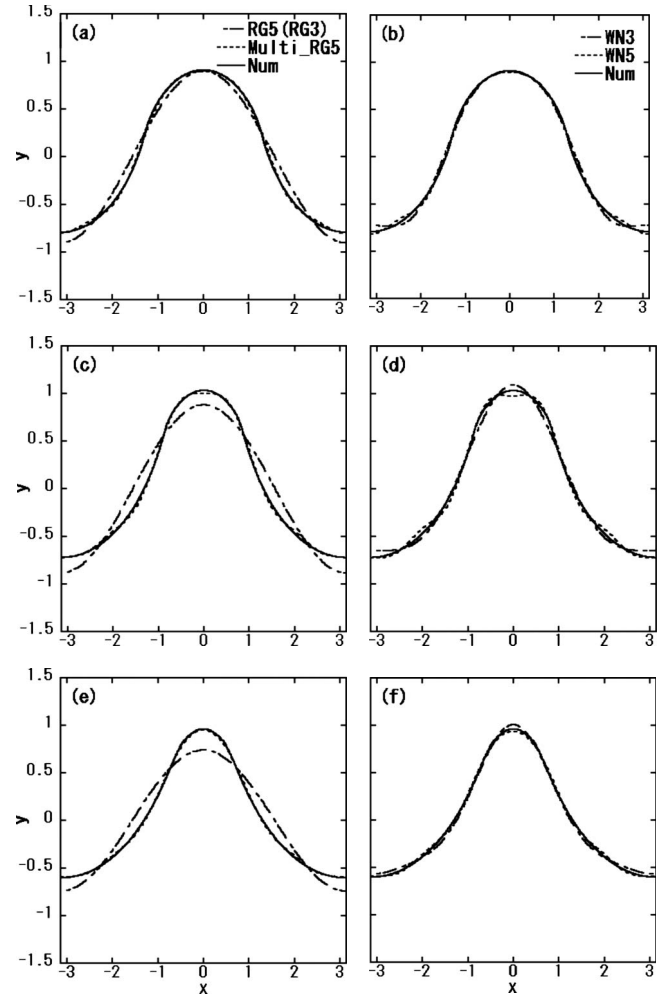


FIG. 3. Interfacial profiles for A =(a) and (b) 0.2, (c) and (d) 0.5, and (e) and (f) 0.7, where $t=0.95$ in (a)–(d) and $t=0.8$ in (e),(f). The dot-dashed and dashed lines in the left-hand-side figures indicate the fifth (third) -order single-mode RG and the fifth-order multimode RG solutions, respectively, and those lines in the right-hand-side figures indicate the third- and fifth-order WN solutions. The solid lines indicate the numerical results. The upper fluid ($y>0$) is assumed to be lighter than the lower one ($y<0$). The numerical calculations in the figure are performed with the same method as in Figs. 1 and 2.

amplitudes in Fig. 1, the results by the multimode RG solution best agree with the numerical calculations in all analytical results.

Figure 3 shows the interfacial profiles at the final (critical) times in Figs. 1 and 2. The third-order single-mode RG solution (RG3) coincides with the fifth-order single-mode RG solution (RG5), at least on the plot. As found in the previous figures, the profiles obtained by the multimode RG solution cannot distinguish from the numerical results. The results by the WN analysis better describes the numerical results than the single-mode RG approach up to this time ($t<1$). From Figs. 1–3, we see that the approximation in the single-mode RG solutions does not increase although we calculate up to the fifth order $O(\tilde{A}(t)^5)$ in Eq. (9).

Figure 4 shows amplitudes and velocities of bubbles and spikes corresponding to Figs. 1 and 2. The numerical calcu-

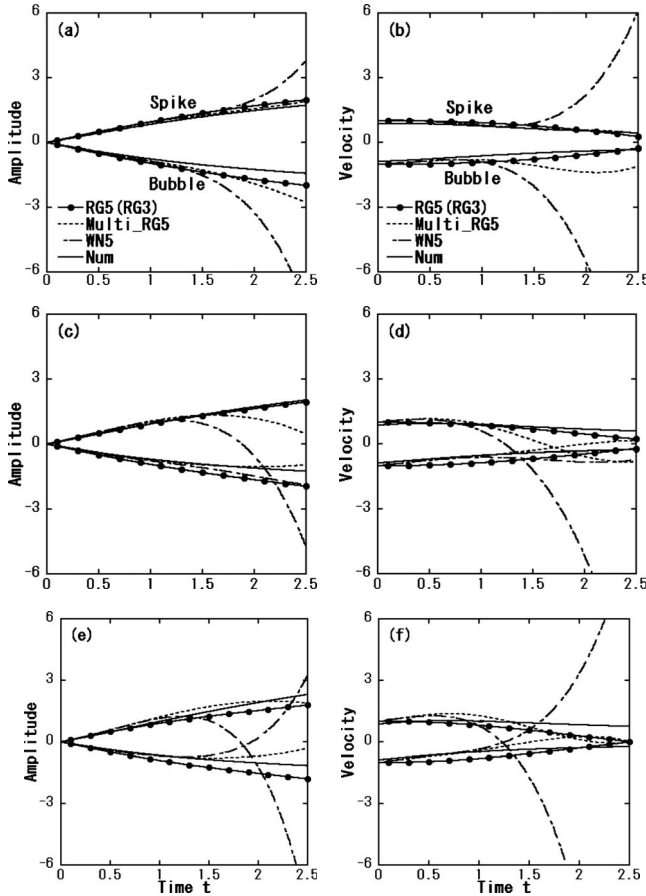


FIG. 4. Amplitudes [(a), (c), and (e)] and velocities [(b), (d), and (f)] of bubbles and spikes for $A=(a)$ and (b) 0.2, (c) and (d) 0.5, and (e) and (f) 0.7, where the solid lines with black circles, dashed, dot-dashed, and solid lines denote the fifth (third) -order single-mode RG, fifth-order multimode RG, fifth-order WN, and numerical solutions, respectively. The numerical calculations in the figure are performed by the vortex method with regularized parameter $\delta=0.1$.

Calculations in the figure are performed by the vortex method with regularized parameter $\delta=0.1$ and the time intervals are taken over $0 \leq t \leq 2.5$ for all calculations. The existence of finite regularized parameter δ ($\delta=0$ in numerical calculations in Figs. 1–3) enables us to perform numerical calculations beyond the Moore’s curvature singularity, i.e., the Kelvin-Helmholtz instability. As stated in the beginning of this section, the obtained solution by this method does not approximate the analytical solution of Eqs. (1) and (2) so accurately as the one used in Figs. 1–3, however, this method describes experimental results relatively well. We see that the single-mode RG solutions fit the numerical solutions pretty well for all Atwood numbers even for $t > 1$ (especially in spike), whereas the WN solutions deviate from the numerical ones and diverge for $t > 1$. The multimode RG solutions also begin to deviate from the numerical results approximately at $t=1.5$.

When $t > 3$, the interface by the numerical calculation with finite δ begins to roll up and the shape loses its univaluedness. Comparison of analytical (RG and WN) amplitudes with the numerical one for $A=0.2$ is presented in Fig. 5(a).

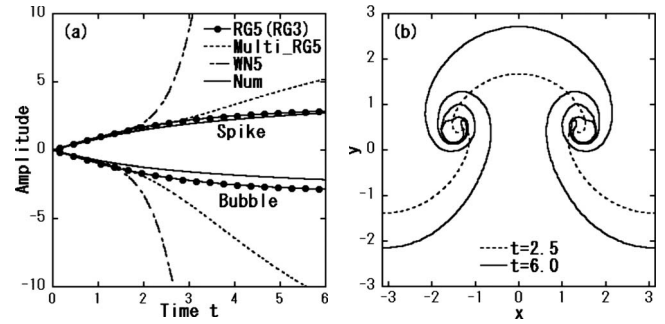


FIG. 5. Comparison of RG approach and numerical results at asymptotic stage for $A=0.2$; (a) amplitudes of bubbles and spikes for $0 \leq t \leq 6.0$, where the solid line with black circles, dashed, dot-dashed, and solid lines denote the fifth (third) -order single-mode RG, fifth-order multimode RG, fifth-order WN, and numerical solutions, respectively, and (b) numerical interfacial profiles at $t=2.5$ (dashed line) and $t=6.0$ (solid line). The numerical calculations are performed by the same method and same δ as in Fig. 4.

When $t > 2$, the multimode RG solution also begins to diverge as well as the WN solution, however, the single-mode RG solution agrees pretty well with the numerical result even at this asymptotic stage, especially in spike. For the sake of reference, we show the numerical interfacial profile at $t=2.5$ and 6.0 in Fig. 5(b). This numerical calculation breaks down at $t=6.2$.

V. CONCLUSION

We have investigated the interfacial motion in RMI in terms of the RG approach. Using this approach, we performed renormalization to the initial amplitude of the potential, B_1 given by the asymptotic linear growth rate v_{lin} and derived an amplitude equation such that the solution is asymptotically nondivergent. We have calculated the RG equation up to the fifth order; however, the results have shown that it is sufficient to perform the calculation up to the third order, at least for the single-mode solution. This single-mode solution describes pretty well the behavior of bubbles and spikes for large t . On the other hand, the multimode RG solution can approximate the analytical solution of the governing equations up to its break-down time, although that cannot describe the asymptotic stage for $t \gg 1$. Using the multimode RG solution, we can obtain better results than those obtained by the WN analysis. These results show that the RG approach is effective for investigating the nonlinear stage in RMI for both of the analytical accuracy ($\delta=0$) and the realistic model with roll-up ($\delta \neq 0$). The solution by the RG approach is not the local solution such as the solution given by the potential-flow model, therefore, that can describe the asymptotic behavior of spikes as well as bubbles. In RMI, there is little difference between the single-mode third-order and fifth-order RG solutions, however, this is not always true for another systems. Similar calculations using the RG approach are possible for the cylindrical case [29,30] and we can obtain a better approximation using the RG

equation than the calculations by the WN analysis [30] for asymptotic interfacial motion.

ACKNOWLEDGMENTS

The author would like to thank Professor K. Nozaki and Professor K. Nishihara for the valuable discussions and their useful comments. This work is partially supported by a Grant-in-Aid for Scientific Research (C) from the Japan Society for the Promotion of Science.

APPENDIX

In this appendix, we derive the fifth-order quantities $\phi_1^{(5)}$ and $\phi_1^{(5)}$ to lead $\eta^{(5)}$ in Eq. (3) in Sec. II. The derivation of the quantities up to the fourth order is identical to that presented in the Appendix in Ref. [9], except the signs of A and ϕ_i ($\mathbf{u}_i = -\nabla \phi_i$ in their definition). For the fifth order $O(\epsilon^5)$, the Bernoulli equation (1) and the kinematic boundary condition [Eq. (2)] yields

$$\begin{aligned}
& (1 - A) \frac{\partial \phi_1^{(5)}}{\partial t} - (1 + A) \frac{\partial \phi_2^{(5)}}{\partial t} \\
&= - (1 - A) \left\{ \sum_{k=2}^4 \frac{\partial^2 \phi_1^{(k)}}{\partial t \partial y} \eta^{(5-k)} + \frac{1}{2} \frac{\partial^3 \phi_1^{(2)}}{\partial t \partial y^2} \sum_{k=1}^2 \eta^{(k)} \eta^{(3-k)} + \frac{1}{2} \frac{\partial^3 \phi_1^{(3)}}{\partial t \partial y^2} (\eta^{(1)})^2 + \frac{1}{3!} \frac{\partial^4 \phi_1^{(2)}}{\partial t \partial y^3} (\eta^{(1)})^3 \right. \\
&+ \frac{\partial \phi_1^{(1)}}{\partial x} \sum_{k=1}^3 \frac{\partial^2 \phi_1^{(k)}}{\partial x \partial y} \eta^{(4-k)} + \frac{\partial \phi_1^{(2)}}{\partial x} \sum_{k=1}^2 \frac{\partial^2 \phi_1^{(k)}}{\partial x \partial y} \eta^{(3-k)} + \frac{\partial \phi_1^{(3)}}{\partial x} \frac{\partial^2 \phi_1^{(1)}}{\partial x \partial y} \eta^{(1)} + \frac{\partial \phi_1^{(3)}}{\partial x} \frac{\partial \phi_1^{(2)}}{\partial x} + \frac{\partial \phi_1^{(4)}}{\partial x} \frac{\partial \phi_1^{(1)}}{\partial x} \\
&+ \frac{1}{2} \frac{\partial \phi_1^{(1)}}{\partial x} \left[\frac{\partial^3 \phi_1^{(1)}}{\partial x \partial y^2} \sum_{k=1}^2 \eta^{(k)} \eta^{(3-k)} + \frac{\partial^3 \phi_1^{(2)}}{\partial x \partial y^2} (\eta^{(1)})^2 \right] + \frac{\partial^2 \phi_1^{(1)}}{\partial x \partial y} \frac{\partial^2 \phi_1^{(2)}}{\partial x \partial y} (\eta^{(1)})^2 + \left(\frac{\partial^2 \phi_1^{(1)}}{\partial x \partial y} \right)^2 \eta^{(1)} \eta^{(2)} \\
&+ \frac{1}{2} \frac{\partial \phi_1^{(2)}}{\partial x} \frac{\partial^3 \phi_1^{(1)}}{\partial x \partial y^2} (\eta^{(1)})^2 + \frac{1}{2} \frac{\partial^2 \phi_1^{(1)}}{\partial x \partial y} \frac{\partial^3 \phi_1^{(1)}}{\partial x \partial y^2} (\eta^{(1)})^3 + \frac{1}{3!} \frac{\partial \phi_1^{(1)}}{\partial x} \frac{\partial^4 \phi_1^{(1)}}{\partial x \partial y^3} (\eta^{(1)})^3 + \frac{\partial \phi_1^{(1)}}{\partial y} \sum_{k=1}^3 \frac{\partial^2 \phi_1^{(k)}}{\partial y^2} \eta^{(4-k)} \\
&+ \frac{\partial \phi_1^{(2)}}{\partial y} \sum_{k=1}^2 \frac{\partial^2 \phi_1^{(k)}}{\partial y^2} \eta^{(3-k)} + \frac{\partial \phi_1^{(3)}}{\partial y} \frac{\partial^2 \phi_1^{(1)}}{\partial y^2} \eta^{(1)} + \frac{\partial \phi_1^{(3)}}{\partial y} \frac{\partial \phi_1^{(2)}}{\partial y} + \frac{\partial \phi_1^{(4)}}{\partial y} \frac{\partial \phi_1^{(1)}}{\partial y} + \frac{1}{2} \frac{\partial \phi_1^{(1)}}{\partial y} \left[\frac{\partial^3 \phi_1^{(1)}}{\partial y^3} \sum_{k=1}^2 \eta^{(k)} \eta^{(3-k)} + \frac{\partial^3 \phi_1^{(2)}}{\partial y^3} (\eta^{(1)})^2 \right] \\
&+ \left. \frac{\partial^2 \phi_1^{(1)}}{\partial y^2} \frac{\partial^2 \phi_1^{(2)}}{\partial y^2} (\eta^{(1)})^2 + \left(\frac{\partial^2 \phi_1^{(1)}}{\partial y^2} \right)^2 \eta^{(1)} \eta^{(2)} + \frac{1}{2} \frac{\partial \phi_1^{(2)}}{\partial y} \frac{\partial^3 \phi_1^{(1)}}{\partial y^3} (\eta^{(1)})^2 + \frac{1}{2} \frac{\partial^2 \phi_1^{(1)}}{\partial y^2} \frac{\partial^3 \phi_1^{(1)}}{\partial y^3} (\eta^{(1)})^3 + \frac{1}{3!} \frac{\partial \phi_1^{(1)}}{\partial y} \frac{\partial^4 \phi_1^{(1)}}{\partial y^4} (\eta^{(1)})^3 \right\} \\
&+ (1 + A) \left\{ \sum_{k=2}^4 \frac{\partial^2 \phi_2^{(k)}}{\partial t \partial y} \eta^{(5-k)} + \frac{1}{2} \frac{\partial^3 \phi_2^{(2)}}{\partial t \partial y^2} \sum_{k=1}^2 \eta^{(k)} \eta^{(3-k)} + \frac{1}{2} \frac{\partial^3 \phi_2^{(3)}}{\partial t \partial y^2} (\eta^{(1)})^2 + \frac{1}{3!} \frac{\partial^4 \phi_2^{(2)}}{\partial t \partial y^3} (\eta^{(1)})^3 \right. \\
&+ \frac{\partial \phi_2^{(1)}}{\partial x} \sum_{k=1}^3 \frac{\partial^2 \phi_2^{(k)}}{\partial x \partial y} \eta^{(4-k)} + \frac{\partial \phi_2^{(2)}}{\partial x} \sum_{k=1}^2 \frac{\partial^2 \phi_2^{(k)}}{\partial x \partial y} \eta^{(3-k)} + \frac{\partial \phi_2^{(3)}}{\partial x} \frac{\partial^2 \phi_2^{(1)}}{\partial x \partial y} \eta^{(1)} + \frac{\partial \phi_2^{(3)}}{\partial x} \frac{\partial \phi_2^{(2)}}{\partial x} + \frac{\partial \phi_2^{(4)}}{\partial x} \frac{\partial \phi_2^{(1)}}{\partial x} \\
&+ \frac{1}{2} \frac{\partial \phi_2^{(1)}}{\partial x} \left[\frac{\partial^3 \phi_2^{(1)}}{\partial x \partial y^2} \sum_{k=1}^2 \eta^{(k)} \eta^{(3-k)} + \frac{\partial^3 \phi_2^{(2)}}{\partial x \partial y^2} (\eta^{(1)})^2 \right] + \frac{\partial^2 \phi_2^{(1)}}{\partial x \partial y} \frac{\partial^2 \phi_2^{(2)}}{\partial x \partial y} (\eta^{(1)})^2 + \left(\frac{\partial^2 \phi_2^{(1)}}{\partial x \partial y} \right)^2 \eta^{(1)} \eta^{(2)} + \frac{1}{2} \frac{\partial \phi_2^{(2)}}{\partial x} \frac{\partial^3 \phi_2^{(1)}}{\partial x \partial y^2} (\eta^{(1)})^2 \\
&+ \frac{1}{2} \frac{\partial^2 \phi_2^{(1)}}{\partial x \partial y} \frac{\partial^3 \phi_2^{(1)}}{\partial x \partial y^2} (\eta^{(1)})^3 + \frac{1}{3!} \frac{\partial \phi_2^{(1)}}{\partial x} \frac{\partial^4 \phi_2^{(1)}}{\partial x \partial y^3} (\eta^{(1)})^3 + \frac{\partial \phi_2^{(1)}}{\partial y} \sum_{k=1}^3 \frac{\partial^2 \phi_2^{(k)}}{\partial y^2} \eta^{(4-k)} + \frac{\partial \phi_2^{(2)}}{\partial y} \sum_{k=1}^2 \frac{\partial^2 \phi_2^{(k)}}{\partial y^2} \eta^{(3-k)} + \frac{\partial \phi_2^{(3)}}{\partial y} \frac{\partial^2 \phi_2^{(1)}}{\partial y^2} \eta^{(1)} \\
&+ \frac{\partial \phi_2^{(3)}}{\partial y} \frac{\partial \phi_2^{(2)}}{\partial y} + \frac{\partial \phi_2^{(4)}}{\partial y} \frac{\partial \phi_2^{(1)}}{\partial y} + \frac{1}{2} \frac{\partial \phi_2^{(1)}}{\partial y} \left[\frac{\partial^3 \phi_2^{(1)}}{\partial y^3} \sum_{k=1}^2 \eta^{(k)} \eta^{(3-k)} + \frac{\partial^3 \phi_2^{(2)}}{\partial y^3} (\eta^{(1)})^2 \right] + \frac{\partial^2 \phi_2^{(1)}}{\partial y^2} \frac{\partial^2 \phi_2^{(2)}}{\partial y^2} (\eta^{(1)})^2 + \left(\frac{\partial^2 \phi_2^{(1)}}{\partial y^2} \right)^2 \eta^{(1)} \eta^{(2)} \\
&+ \left. \frac{1}{2} \frac{\partial \phi_2^{(2)}}{\partial y} \frac{\partial^3 \phi_2^{(1)}}{\partial y^3} (\eta^{(1)})^2 + \frac{1}{2} \frac{\partial^2 \phi_2^{(1)}}{\partial y^2} \frac{\partial^3 \phi_2^{(1)}}{\partial y^3} (\eta^{(1)})^3 + \frac{1}{3!} \frac{\partial \phi_2^{(1)}}{\partial y} \frac{\partial^4 \phi_2^{(1)}}{\partial y^4} (\eta^{(1)})^3 \right\} \tag{A1}
\end{aligned}$$

and the kinematic boundary condition Eq. (2) becomes

$$\begin{aligned}
 \frac{\partial \eta^{(5)}}{\partial t} - \frac{\partial \phi_i^{(5)}}{\partial y} = & - \left[\sum_{k=1}^4 \frac{\partial \phi_i^{(k)}}{\partial x} \frac{\partial \eta^{(5-k)}}{\partial x} + \sum_{k=1}^3 \frac{\partial^2 \phi_i^{(k)}}{\partial x \partial y} \frac{\partial \eta^{(4-k)}}{\partial x} \eta^{(1)} + \sum_{k=1}^2 \frac{\partial^2 \phi_i^{(k)}}{\partial x \partial y} \frac{\partial \eta^{(3-k)}}{\partial x} \eta^{(2)} + \frac{\partial^2 \phi_i^{(1)}}{\partial x \partial y} \frac{\partial \eta^{(1)}}{\partial x} \eta^{(3)} \right. \\
 & + \frac{1}{2} \sum_{k=1}^2 \frac{\partial^3 \phi_i^{(k)}}{\partial x \partial y^2} \frac{\partial \eta^{(3-k)}}{\partial x} (\eta^{(1)})^2 + \frac{1}{2} \frac{\partial^3 \phi_i^{(1)}}{\partial x \partial y^2} \frac{\partial \eta^{(1)}}{\partial x} \sum_{k=1}^2 \eta^{(k)} \eta^{(3-k)} + \frac{1}{3!} \frac{\partial^4 \phi_i^{(1)}}{\partial x \partial y^3} \frac{\partial \eta^{(1)}}{\partial x} (\eta^{(1)})^3 \left. \right] + \sum_{k=1}^4 \frac{\partial^2 \phi_i^{(k)}}{\partial y^2} \eta^{(5-k)} \\
 & + \frac{1}{2} \frac{\partial^3 \phi_i^{(1)}}{\partial y^3} \sum_{k=1}^3 \eta^{(k)} \eta^{(4-k)} + \frac{1}{2} \frac{\partial^3 \phi_i^{(2)}}{\partial y^3} \sum_{k=1}^2 \eta^{(k)} \eta^{(3-k)} + \frac{1}{2} \frac{\partial^3 \phi_i^{(3)}}{\partial y^3} (\eta^{(1)})^2 + \frac{1}{2} \frac{\partial^4 \phi_i^{(1)}}{\partial y^4} (\eta^{(1)})^2 \eta^{(2)} + \frac{1}{3!} \frac{\partial^4 \phi_i^{(2)}}{\partial y^4} (\eta^{(1)})^3 \\
 & + \frac{1}{4!} \frac{\partial^5 \phi_i^{(1)}}{\partial y^5} (\eta^{(1)})^4 \quad (i = 1, 2).
 \end{aligned}
 \tag{A2}$$

From Eqs. (A1) and (A2), we obtain the fifth-order quantities $\phi_i^{(5)}$ and $\phi_2^{(5)}$,

$$\begin{aligned}
 \phi_1^{(5)}(x, t) = & \left\{ \left[\left(\frac{A^4}{12} + \frac{A^3}{3} + \frac{A^2}{4} - \frac{5A}{24} - \frac{1}{24} \right) B_1^5 k^8 t^4 + a_0 \left(\frac{2A^3}{3} + \frac{2A^2}{3} - \frac{A}{2} - \frac{1}{6} \right) B_1^4 k^7 t^3 \right] \cos kx \right\} e^{-ky} \\
 & + \left\{ \left[\left(-\frac{9A^4}{8} + \frac{A^3}{24} + \frac{55A^2}{32} - \frac{29A}{48} - \frac{7}{96} \right) B_1^5 k^8 t^4 + \left(-\frac{2A^3}{3} + \frac{65A^2}{24} - \frac{17A}{12} - \frac{7}{24} \right) B_1^4 k^7 t^3 \right] \cos 3kx \right\} e^{-3ky} \\
 & + \left\{ \left[\left(\frac{25A^4}{24} - \frac{55A^3}{24} + \frac{151A^2}{96} - \frac{5A}{16} - \frac{1}{96} \right) B_1^5 k^8 t^4 + a_0 \left(-\frac{4A^3}{3} + \frac{17A^2}{8} - \frac{3A}{4} - \frac{1}{24} \right) B_1^4 k^7 t^3 \right] \cos 5kx \right\} e^{-5ky} \quad (y > 0), \\
 \phi_2^{(5)}(x, t) = & \left\{ \left[\left(-\frac{A^4}{12} + \frac{A^3}{3} - \frac{A^2}{4} - \frac{5A}{24} + \frac{1}{24} \right) B_1^5 k^8 t^4 + a_0 \left(\frac{2A^3}{3} - \frac{2A^2}{3} - \frac{A}{2} + \frac{1}{6} \right) B_1^4 k^7 t^3 \right] \cos kx \right\} e^{ky} \\
 & + \left\{ \left[\left(\frac{9A^4}{8} + \frac{A^3}{24} - \frac{55A^2}{32} - \frac{29A}{48} + \frac{7}{96} \right) B_1^5 k^8 t^4 + \left(-\frac{2A^3}{3} - \frac{65A^2}{24} - \frac{17A}{12} + \frac{7}{24} \right) B_1^4 k^7 t^3 \right] \cos 3kx \right\} e^{3ky} \\
 & + \left\{ \left[\left(-\frac{25A^4}{24} - \frac{55A^3}{24} - \frac{151A^2}{96} - \frac{5A}{16} + \frac{1}{96} \right) B_1^5 k^8 t^4 + a_0 \left(-\frac{4A^3}{3} - \frac{17A^2}{8} - \frac{3A}{4} + \frac{1}{24} \right) B_1^4 k^7 t^3 \right] \cos 5kx \right\} e^{5ky} \quad (y < 0),
 \end{aligned}
 \tag{A3}$$

where we dropped the terms proportional to t^2 in $\phi_i^{(5)}$ ($i=1, 2$).

[1] R. D. Richtmyer, *Commun. Pure Appl. Math.* **13**, 297 (1960); E. E. Meshkov, *Fluid Dyn.* **4**, 101 (1969).
 [2] Y. Andreopoulos, J. H. Agui, and G. Briassulis, *Rev. Fluid Mech.* **32**, 309 (2000).
 [3] S. I. Abarzhi, *Phys. Scr., T* **132**, 014012 (2008); S. I. Abarzhi and K. R. Sreenivasan, *Philos. Trans. R. Soc. London, Ser. A* **368**, 1539 (2010).
 [4] A. L. Velikovich *et al.*, *Phys. Plasmas* **7**, 1662 (2000), and references therein.
 [5] J. G. Wouchuk, *Phys. Rev. E* **63**, 056303 (2001).
 [6] K. Nishihara, J. G. Wouchuk, C. Matsuoka, R. Ishizaki, and V. V. Zhakhovsky, *Philos. Trans. R. Soc. London, Ser. A* **368**, 1769 (2010), and many references therein.
 [7] C. Matsuoka, K. Nishihara and Y. Fukuda, *Phys. Rev. E* **67**, 036301 (2003); **68**, 029902(E) (2003).
 [8] C. Matsuoka and K. Nishihara, *Phys. Rev. E* **73**, 026304 (2006), and references therein; **74**, 049902(E) (2006).
 [9] Q. Zhang and S. Sohn, *Phys. Fluids* **9**, 1106 (1997).
 [10] M. Vandenboomgaerde, S. Gauthier, and C. Mügler, *Phys. Fluids* **14**, 1111 (2002).
 [11] P. Concus, *J. Fluid Mech.* **14**, 568 (1962).
 [12] C. Matsuoka, *Phys. Fluids* **21**, 092107 (2009).
 [13] J. W. Jacobs and V. V. Krivets, *Phys. Fluids* **17**, 034105 (2005).
 [14] For example, V. Hakim, in *Hydrodynamics and Nonlinear Instabilities*, edited by C. Godréche and P. Manneville (Cambridge University Press, Cambridge, 1998), p. 295.
 [15] A. C. Newell and J. A. Whitehead, *J. Fluid Mech.* **38**, 279 (1969).
 [16] T. Kunihiro, *Prog. Theor. Phys.* **94**, 503 (1995).
 [17] L.-Y. Chen, N. Goldenfeld, and Y. Oono, *Phys. Rev. Lett.* **73**, 1311 (1994); *Phys. Rev. E* **54**, 376 (1996).
 [18] K. Nozaki and Y. Oono, *Phys. Rev. E* **63**, 046101 (2001).
 [19] Y. Nambu and Y. Y. Yamaguchi, *Phys. Rev. D* **60**, 104011 (1999).
 [20] S. Goto, Y. Masutomi, and K. Nozaki, *Prog. Theor. Phys.* **102**, 471 (1999).
 [21] V. N. Goncharov, *Phys. Rev. Lett.* **88**, 134502 (2002).
 [22] S.-I. Sohn, *Phys. Rev. E* **67**, 026301 (2003).
 [23] D. Layzer, *Astrophys. J.* **122**, 1 (1955).
 [24] J. G. Wouchuk and K. Nishihara, *Phys. Plasmas* **3**, 3761 (1996); **4**, 1028 (1997).

- [25] H. Chiba, *J. Math. Phys.* **49**, 102703 (2008); H. Chiba and M. Iwasa, *ibid.* **50**, 042703 (2009).
- [26] M. Vandenboomgaerde, C. Boudesocque-Dubois, J. Griffond, and M. Boulet, in *Proceedings of the 10th IWPCTM*, Paris, France, edited by M. Legrand (unpublished), p. 383.
- [27] R. Krasny, *J. Fluid Mech.* **184**, 123 (1987).
- [28] D. W. Moore, *Proc. R. Soc. London* **365**, 105 (1979).
- [29] C. Matsuoka and K. Nishihara, *Phys. Rev. E* **73**, 055304(R) (2006).
- [30] C. Matsuoka and K. Nishihara, *Phys. Rev. E* **74**, 066303 (2006).